XII International Conference on Computational Plasticity. Fundamentals and Applications
COMPLAS XII
E. Oñate, D.R.J. Owen, D. Peric and B. Suárez (Eds)

FE^2-HOMOGENIZATION OF MICROMORPHIC ELASTO-PLASTIC MATERIALS

Heiko Clasen[*,†], **C. Britta Hirschberger**[†], **Jože Korelc**[††] **and Peter Wriggers**[†]

[†]Institute of Continuum Mechanics
Gottfried Wilhelm Leibniz Universität Hannover
Appelstraße 11, 30167 Hanover, Germany
e-mail: clasen@ikm.uni-hannover.de, web page: http://www.ikm.uni-hannover.de

[††]Faculty of Civil and Geodetic Engineering
University of Ljubljana
Jamova 2, SI-1000 Ljubljana, Slovenia
email: jkorelc@fgg.uni-lj.si, web page: http://www.fgg.uni-lj.si/Symech

Key words: Finite Plasticity, Micromorphic Continua, Size–Effects, FE^2, Homogenization

Abstract. In this work, a homogenization strategy for a micromorphic–type inelastic material is presented. In the spirit of FE^2, a representative volume element is attached to each macroscopic quadrature point. Due to the inherent length scale of the micromorphic continuum, size effects for inelastic behavior are obtained on RVE–level. A focus is placed on the computation of the homogenized algorithmic tangent. It is determined via sensitivity analyses with respect to the boundary conditions imposed on the RVE. Following this procedure, costly single–scale computations with dense meshes can be replaced by a robust homogenization approach with optimal convergence rates.

1 INTRODUCTION

Since the beginning of micromechanical analyses by Voigt [1] over a century ago, many analytical approaches to homogenization of inhomogeneous materials were developed (see [2] for an overview). Within the recent decades, increasing computational power lead to a multitude of computational multiscale methods, enabling predictions of the behavior of microscopically heterogeneous materials. Among these methods, the computational homogenization called FE^2 by Miehe et al. [3], [4], Féyel [5] and Féyel and Chaboche [6] has proven especially handy for Finite–Element analyses.

Boundary value problems are computed on RVE–level and the stress response as well as the constitutive tangent are homogenized over the volume and are used in the quadrature point on the macrolevel. In this procedure, the tangent computation is a particularly

challenging point because of the history dependence in the case of an inelastic material. The evolution equations for the inelastic quantities are numerically integrated in time (see [7]). This results in an algorithmic tangent replacing the constitutive tangent on the RVE–level. To achieve optimal macroscopic convergence rates in the homogenization framework, the algorithmic tangent on RVE–level has to be homogenized correctly. In the present solution procedure, we homogenize the algorithmic tangent by a sensitivity analysis regarding the boundary conditions imposed on the RVE as described in the work of Korelc [8] based on the work of Michaleris et al. [9].

On the RVE–level, we want to model a material exhibiting size effects. For this, a formulation including an inner length scale is necessary. Among various gradient–based theories (see [10] for an overview), the micromorphic model documented in Eringen [11] is able to predict size effects. This model was applied to inelastic deformations by Forest [12] and extended to finite deformations by Clasen and Hirschberger [13]: An additional scalar field describing a plastic microdeformation which renders size effects (and mesh regularization in the case of softening) is introduced and treated as a micromorphic degree of freedom. This type of material induces higher–order stresses contributing to the internal work. Thus, the classical Hill–Mandel criterion [14] ensuring an energetically consistent meso–to–macro transition is extended in the sense of Hirschberger et al. [15] to a micromorphic–type mesostructure in the RVE.

As a result, a numerical homogenization framework with an optimal convergence rate for a finite–deformation elasto–plastic material exhibiting size effects on RVE–level (and consequently in the mechanical overall–response) is obtained.

2 CONTINUUM MECHANICAL MULTISCALE FRAMEWORK

To set the stage for the homogenization procedure, the continuum mechanics of micromorphic–type plasticity used on the mesoscale is reviewed. Afterwards, the governing equations for the macroscale are described. Further on, proper boundary conditions on RVE–level for an energetically consistent meso–to–macro transition are developed.

2.1 Mesoscale

In this section, the general framework for micromorphic–type elasto–plasticity is derived. Hyperelasto–plastic material behavior on the mesolevel is accompanied by an additional regularizing degree of freedom governed by its own partial differential equation. In the terminology of micromorphic continua, this degree of freedom is referred to as plastic micro–deformation.

The micromorphic elasto–plastic formulation is similar to standard plasticity. The deformation gradient $\boldsymbol{F}$ is split into an elastic part $\boldsymbol{F}^e$ and a plastic part $\boldsymbol{F}^p$:

$$\boldsymbol{F} = \frac{\partial \boldsymbol{x}}{\partial \boldsymbol{X}} = \boldsymbol{F}^e \cdot \boldsymbol{F}^p \tag{1}$$

$$J = \det \boldsymbol{F} \tag{2}$$

With this, the elastic left Cauchy–Green–tensor $\boldsymbol{b}^e$ can be calculated as follows:

$$\boldsymbol{b}^e = \boldsymbol{F}^e \cdot (\boldsymbol{F}^e)^T = \boldsymbol{F} \cdot (\boldsymbol{C}^p)^{-1} \cdot \boldsymbol{F}^T \tag{3}$$

The difference to the standard model is the presence of an additional scalar field $\bar{\alpha}$ representing the plastic micro–deformation. This field is comparable to the equivalent plastic strain on the mesoscale. In the following section, not only $\bar{\alpha}$, but also its gradient with respect to the reference configuration $\nabla\bar{\alpha}$ are used.

With the kinematics at hand, we introduce the kinetics starting with the formulation of a free energy density function Ψ. This function depends on the set of state variables $\{\boldsymbol{b}^e, \bar{\alpha}, \nabla\bar{\alpha}\}$. Due to the inelastic material behavior, the strain energy density also depends on the internal variables $\{\boldsymbol{\xi}\}$.

$$\Psi = \Psi(\boldsymbol{b}^e, \bar{\alpha}, \nabla\bar{\alpha}; \boldsymbol{\xi}) \tag{4}$$

Now, the internal stress power is compared to the total rate of the free energy density, which gives an inequality for the internal dissipation $\mathcal{D}$:

$$\mathcal{D} = \boldsymbol{\tau} : \boldsymbol{l} + a\dot{\bar{\alpha}} + \boldsymbol{b} \cdot \nabla\dot{\bar{\alpha}} - \dot{\Psi} \geq 0 \tag{5}$$

The internal stress power has three contributions: $\boldsymbol{\tau}$ is the Kirchhoff stress tensor corresponding to the the spatial velocity gradient $\boldsymbol{l}$. a and $\boldsymbol{b}$ are called couple stress and double stress respectively corresponding to the rate of the plastic micro–deformation and its gradient.

Inserting the rate of the free energy density $\dot{\Psi}$ into the dissipation inequality, the definitions for the stresses $\boldsymbol{\tau}$, a and $\boldsymbol{b}$ are obtained:

$$\boldsymbol{\tau} = 2\frac{\partial\Psi}{\partial\boldsymbol{b}^e} \cdot \boldsymbol{b}^e \tag{6}$$

$$a = \frac{\partial\Psi}{\partial\bar{\alpha}} \tag{7}$$

$$\boldsymbol{b} = \frac{\partial\Psi}{\partial\nabla\bar{\alpha}} \tag{8}$$

Additionally, the power–conjugate driving force for the evolution of the internal variables can be determined:

$$\boldsymbol{h} = \frac{\partial\Psi}{\partial\boldsymbol{\xi}} \tag{9}$$

Then, the dissipation inequality reduces to

$$\mathcal{D} = \boldsymbol{\tau} : \left(-\frac{1}{2}\mathcal{L}_\nu \boldsymbol{b}^e \cdot (\boldsymbol{b}^e)^{-1}\right) - \boldsymbol{h} \cdot \dot{\boldsymbol{\xi}} \geq 0 \tag{10}$$

To determine the stresses, a constitutive formulation on the mesoscale is required. For a simple and convenient description of the material model, the free energy density is split into two parts:

$$\Psi = \Psi_{meso} + \Psi_{micro} \tag{11}$$

For the mesoscopic part Ψ_{meso} depending on $\{\boldsymbol{b}^e; \boldsymbol{\xi}\}$, a neo–Hookean free energy density is used:

$$\Psi_{meso} = \frac{\mu}{2}\left(\mathrm{Tr}(\boldsymbol{b}^e) - 3\right) - \mu \ln J + \frac{\lambda}{4}\left(J^2 - 2\ln J - 1\right) + \frac{1}{2}K\alpha^2 \tag{12}$$

It is obvious, that the first three terms describe the stored elastic energy depending on the Lamé–constants μ and λ. The fourth term is responsible for the hardening, where we restrict ourselves to linear isotropic hardening described by the accumulated plastic strain α and the hardening modulus K.

As proposed by Forest [12], the regularizing part of the free energy density Ψ_{micro} depending on $\{\bar{\alpha}, \nabla\bar{\alpha}; \alpha\}$ and the material parameters H and A is chosen as

$$\Psi_{micro} = \frac{1}{2}H\left(\alpha - \bar{\alpha}\right)^2 + \frac{1}{2}A\,\nabla\bar{\alpha}\cdot\nabla\bar{\alpha} \tag{13}$$

Once the strain energy density is known, the stresses can be determined according to eqs. (6)–(8).

The inelastic part of the deformation is described by a J_2–plasticity model assuming maximum plastic dissipation. Thus, the yield condition Φ for the onset of plasticity can be written as

$$\Phi = \tau_{vM} - (\tau_y + h) \leq 0 \tag{14}$$

with the von–Mises–stress τ_{vM}, the initial yield stress τ_y and the hardening function h which is scalar in the case of isotropic hardening as the only entry in $\boldsymbol{\xi}$ is the equivalent plastic strain α. This means that

$$h = \frac{\partial\Psi}{\partial\alpha} = K\alpha + H(\alpha - \bar{\alpha}) \tag{15}$$

At this point, the additional micro–deformation $\bar{\alpha}$ enters the mesoscale.

As associative elasto–plasticity is considered, the yield condition is now used as the plastic potential in the flow rule which includes the plastic multiplier $\dot{\gamma}$:

$$-\frac{1}{2}\mathcal{L}_\nu\boldsymbol{b}^e\cdot(\boldsymbol{b}^e)^{-1} = \dot{\gamma}\frac{\partial\Phi}{\partial\boldsymbol{\tau}} \tag{16}$$

This evolution equation is solved with the exponential mapping of Simo [7]. Also, an evolution equation for the equivalent plastic strain can be determined:

$$\dot{\alpha} = \dot{\gamma} \tag{17}$$

The Kirchhoff–stresses $\boldsymbol{\tau}$ as well as the couple- and double–stresses a and $\boldsymbol{b}$ have to fulfill their respective equilibrium equations. For the mesolevel, this is the standard balance of linear momentum. In terms of the first Piola–Kirchhoff–stresses $\boldsymbol{P} = \boldsymbol{\tau}\cdot\boldsymbol{F}^{-T}$, this balance can be written as

$$\mathrm{Div}(\boldsymbol{P}) = \boldsymbol{0} \tag{18}$$

where quasistatic loading is assumed and body forces are neglected. This equilibrium equation is accompanied by proper boundary conditions for the displacement boundary $\partial\Omega^{\boldsymbol{u}}$ and the traction boundary $\partial\Omega^{\boldsymbol{t}}$. In general, these can be written as

$$\boldsymbol{u} = \boldsymbol{u}^{pre} \quad \text{on} \quad \partial\Omega^{\boldsymbol{u}} \tag{19}$$

$$\boldsymbol{t}_0^{pre} = \boldsymbol{P} \cdot \boldsymbol{N} \quad \text{on} \quad \partial\Omega^{\boldsymbol{t}} \tag{20}$$

where $\boldsymbol{u}^{pre}$ are the prescribed displacements, $\boldsymbol{t}_0^{pre}$ are the prescribed tractions in the reference configuration and $\boldsymbol{N}$ is the outward normal in the reference configuration.

For the microdeformation, the balance of microforces leads to the following equation:

$$\mathrm{Div}(\boldsymbol{b}) = a \tag{21}$$

According to the choice of Ψ_{micro} the following partial differential equation can be obtained:

$$\bar{\alpha} - \frac{A}{H}\nabla^2\bar{\alpha} = \alpha \tag{22}$$

For this equation, no prescribed Dirichlet boundary conditions on the boundary $\partial\Omega^{\bar{\alpha}}$ are assumed. For the Neumann boundary $\partial\Omega^{\boldsymbol{b}}$, normality conditions in the following form are assumed:

$$\boldsymbol{b} \cdot \boldsymbol{N} = 0 \quad \text{on} \quad \partial\Omega^{\boldsymbol{b}} \tag{23}$$

2.2 Macroscale

On the macrolevel, the kinematics of standard nonlinear continuum mechanics are used:

$$\widehat{\boldsymbol{F}} = \frac{\partial\widehat{\boldsymbol{x}}}{\partial\widehat{\boldsymbol{X}}} \tag{24}$$

Contrary to the mesolevel, no a–priori constitutive assumption is made on this level. Instead, the homogenized stress $\widehat{\boldsymbol{P}}$ obtained by

$$\widehat{\boldsymbol{P}} = \frac{1}{V}\int \boldsymbol{P}\mathrm{d}\Omega \tag{25}$$

is used. The tangent $\widehat{\boldsymbol{A}}$, defined by

$$\widehat{\boldsymbol{A}} = \frac{\mathrm{D}\widehat{\boldsymbol{P}}}{\mathrm{D}\widehat{\boldsymbol{F}}} \tag{26}$$

has to be evaluated numerically as it depends on the history–variables and the algorithm for numerical time–integration to determine those variables. The determination of this tangent will be described in section 3. Once this tangent is known, the macroequilibrium $\mathrm{Div}\widehat{\boldsymbol{P}} = \boldsymbol{0}$ can be solved by the minimization of a pseudo–potential Ψ_{macro}:

$$\int \Psi_{macro}\mathrm{d}\widehat{\Omega} = \int \widehat{\boldsymbol{P}} : \widehat{\boldsymbol{F}}\mathrm{d}\widehat{\Omega} \rightarrow \min \tag{27}$$

2.3 Meso–to–macro transition

A meso–to–macro transition can only be physically meaningful, if the virtual work on the mesolevel equals the virtual work on the macrolevel. This criterion is known as the Hill–Mandel criterion (see [14]). Due to the micromorphic–type continuum, this criterion has to be extended, such that not only $\boldsymbol{P}$ but also the contributions of the stresses a and $\boldsymbol{b}$ are taken into account [15]. In the underlying case, this criterion can be written as follows:

$$\widehat{\boldsymbol{P}} : \delta\widehat{\boldsymbol{F}} = \frac{1}{V}\int (\boldsymbol{P} : \delta\boldsymbol{F} + a\delta\bar{\alpha} + \boldsymbol{b}\cdot\delta\nabla\bar{\alpha})\mathrm{d}\Omega \tag{28}$$

In general, different types of boundary conditions can be applied to ensure relation (28). In this work, periodic boundary conditions are chosen. The placement in the current configuration $\boldsymbol{x}$ can be expressed by the average deformation gradient $\widehat{\boldsymbol{F}}$ and a fluctuation $\tilde{\boldsymbol{x}}$ in the following way:

$$\boldsymbol{x} = \widehat{\boldsymbol{F}}\cdot\boldsymbol{X} + \tilde{\boldsymbol{x}} \tag{29}$$

The microfluctuation can be seen figure 1, where the linear displacement boundary condi-

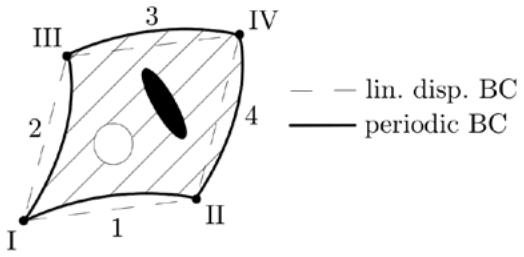

Figure 1: Boundary conditions on RVE–level

tions $\boldsymbol{x} = \widehat{\boldsymbol{F}}\cdot\boldsymbol{X}$ are shown additionally to the periodic boundary conditions. For a better understanding, the boundary of the RVE is split into two parts: $\partial\Omega^+$ and $\partial\Omega^-$ which describe the "positive" and the "negative" part of the boundary respectively. Using the denomination in figure 1, the edges indicated with the numbers 1 and 2 are considered as the positive boundary, whereas the edges 3 and 4 are the negative boundary. To ensure periodicity, the following constraint must be fulfilled by the fluctuation field:

$$\tilde{\boldsymbol{x}}^+ = \tilde{\boldsymbol{x}}^- \tag{30}$$

Together with antiperiodic tractions

$$\boldsymbol{t_0}^+ = -\boldsymbol{t_0}^- \tag{31}$$

it can be shown, that the virtual work criterion is fulfilled. From equation (28) it can be deduced that

$$\widehat{\boldsymbol{P}} : \delta\widehat{\boldsymbol{F}} = \frac{1}{V}\int \boldsymbol{P} : \delta\boldsymbol{F}\mathrm{d}\Omega + \frac{1}{V}\int (a\delta\bar{\alpha} + \boldsymbol{b}\cdot\delta\nabla\bar{\alpha})\mathrm{d}\Omega \tag{32}$$

By applying the Gauss-theorem, we find that the second integral on the right–hand–side vanishes due to the choice of the normality Neumann boundary conditions on the micro–level:

$$\frac{1}{V}\int (a\delta\bar{\alpha} + \boldsymbol{b}\cdot\delta\nabla\bar{\alpha})\mathrm{d}\Omega = 0 \tag{33}$$

Thus, the equation which has to be fulfilled to ensure an energetically consistent homogenization is

$$\widehat{\boldsymbol{P}} : \delta\widehat{\boldsymbol{F}} = \frac{1}{V}\int \boldsymbol{P} : \delta\boldsymbol{F}\mathrm{d}\Omega \tag{34}$$

The proof that periodic boundary conditions fulfill this equation can be found in the literature, e.g. [16].

Within the Finite–Element analysis, the deformation gradient $\widehat{\boldsymbol{F}}$ obtained from the macrolevel is applied on the corner nodes 1, 2 and 3 (see figure 1). To ensure periodicity, constraint elements are added on the boundary to couple the displacement $\boldsymbol{u}$ as well as the plastic microdeformation $\bar{\alpha}$ on the edges 1–3 and 2–4 respectively via the augmented Lagrange method.

3 NUMERICAL MULTISCALE FRAMEWORK

The choice of boundary conditions allows to determine the exact homogenized material tangent used on the macrolevel by sensitivity analyses accompanying the computation of the primary degrees of freedom. The homogenized material tangent $\widehat{\boldsymbol{A}}$ with

$$\widehat{\boldsymbol{A}} = \frac{\mathrm{D}\widehat{\boldsymbol{P}}}{\mathrm{D}\widehat{\boldsymbol{F}}} = \frac{1}{V}\int \frac{\mathrm{D}\boldsymbol{P}}{\mathrm{D}\widehat{\boldsymbol{F}}}\mathrm{d}\Omega \tag{35}$$

is necessary to solve the macroequilibrium $\mathrm{Div}\widehat{\boldsymbol{P}} = \boldsymbol{0}$ by minimization of the macroscopic potential (see (27)). For this, the residual on element level of a Newton–Raphson iteration loop is determined by:

$$\widehat{\boldsymbol{R}}_e = \int \widehat{\boldsymbol{P}} : \frac{\partial\widehat{\boldsymbol{F}}}{\partial\widehat{\boldsymbol{p}}_e}\mathrm{d}\widehat{\Omega} \tag{36}$$

with the vector of degrees of freedom on element level $\widehat{\boldsymbol{p}}_e$. The element tangent matrix is then obtained by computing

$$\widehat{\boldsymbol{K}}_e = \frac{\mathrm{D}\boldsymbol{R}_e(\widehat{\boldsymbol{P}}(\widehat{\boldsymbol{F}}), \widehat{\boldsymbol{F}}(\widehat{\boldsymbol{p}}_e), \widehat{\boldsymbol{p}}_e)}{\mathrm{D}\widehat{\boldsymbol{p}}_e} = \frac{\partial\widehat{\boldsymbol{R}}_e}{\partial\widehat{\boldsymbol{p}}_e} + \frac{\partial\widehat{\boldsymbol{R}}_e}{\partial\widehat{\boldsymbol{P}}}\cdot\frac{\mathrm{D}\widehat{\boldsymbol{P}}}{\mathrm{D}\widehat{\boldsymbol{F}}}\cdot\frac{\partial\widehat{\boldsymbol{F}}}{\partial\widehat{\boldsymbol{p}}_e} = \frac{\partial\widehat{\boldsymbol{R}}_e}{\partial\widehat{\boldsymbol{p}}_e} + \frac{\partial\widehat{\boldsymbol{R}}_e}{\partial\widehat{\boldsymbol{P}}}\cdot\widehat{\boldsymbol{A}}\cdot\frac{\partial\widehat{\boldsymbol{F}}}{\partial\widehat{\boldsymbol{p}}_e} \tag{37}$$

For the computation of the correct material tangent $\widehat{\boldsymbol{A}}$, it is crucial to determine the derivative $\mathrm{D}\boldsymbol{P}/\mathrm{D}\widehat{\boldsymbol{F}}$ (see eq. (35)):

$$\frac{\mathrm{D}\boldsymbol{P}(\widehat{\boldsymbol{F}}(\boldsymbol{p}_e,\boldsymbol{h}_g),\boldsymbol{p}_e,\boldsymbol{h}_g)}{\mathrm{D}\widehat{\boldsymbol{F}}} = \frac{\partial \boldsymbol{P}}{\partial \widehat{\boldsymbol{F}}} + \frac{\partial \boldsymbol{P}}{\partial \boldsymbol{p}_e}\cdot\frac{\mathrm{D}\boldsymbol{p}_e}{\mathrm{D}\widehat{\boldsymbol{F}}} + \frac{\partial \boldsymbol{P}}{\partial \boldsymbol{h}_g}\cdot\frac{\mathrm{D}\boldsymbol{h}_g}{\mathrm{D}\widehat{\boldsymbol{F}}} \tag{38}$$

In this equation, the quantities $\boldsymbol{p}_e$ and $\boldsymbol{h}_g$ denote the vector of degrees of freedom within a finite element and the vector of history variables of the quadrature points in the element respectively. According to [8] and [9], the dependencies occuring in the equation above are determined via sensitivity analyses.

In a converged state, the finite element fulfills the following equations for the independent residual of the degrees of freedom ${}^{n+1}\boldsymbol{R}_e$ and the dependent residual ${}^{n+1}\boldsymbol{Q}$ of the history variables:

$${}^{n+1}\boldsymbol{R}_e({}^{n+1}\boldsymbol{p}_e, {}^{n+1}\boldsymbol{h}_g({}^{n+1}\boldsymbol{p}_e), {}^{n}\boldsymbol{p}_e, {}^{n}\boldsymbol{h}_g) = \boldsymbol{0} \tag{39}$$

$${}^{n+1}\boldsymbol{Q}({}^{n+1}\boldsymbol{p}_e, {}^{n+1}\boldsymbol{h}_g({}^{n+1}\boldsymbol{p}_e), {}^{n}\boldsymbol{p}_e, {}^{n}\boldsymbol{h}_g) = \boldsymbol{0} \tag{40}$$

In the follwing, the superscript ${}^{n+1}$ will be dropped for brevity. To determine the dependency $\mathrm{D}\boldsymbol{p}_e/\mathrm{D}\widehat{\boldsymbol{F}}$, the total derivative of the residual $\boldsymbol{R}_e$ with respect to $\widehat{\boldsymbol{F}}$ is computed:

$$\frac{\partial \boldsymbol{R}_e}{\partial \boldsymbol{p}_e}\frac{\mathrm{D}\boldsymbol{p}_e}{\mathrm{D}\widehat{\boldsymbol{F}}} + \frac{\partial \boldsymbol{R}_e}{\partial \boldsymbol{h}_g}\frac{\mathrm{D}\boldsymbol{h}_g}{\mathrm{D}\widehat{\boldsymbol{F}}} + \frac{\partial \boldsymbol{R}_e}{\partial {}^{n}\boldsymbol{p}_e}\frac{\mathrm{D}^{n}\boldsymbol{p}_e}{\mathrm{D}\widehat{\boldsymbol{F}}} + \frac{\partial \boldsymbol{R}_e}{\partial {}^{n}\boldsymbol{h}_g}\frac{\mathrm{D}^{n}\boldsymbol{h}_g}{\mathrm{D}\widehat{\boldsymbol{F}}} + \frac{\partial \boldsymbol{R}_e}{\partial \widehat{\boldsymbol{F}}} = \boldsymbol{0} \tag{41}$$

From this equation, the derivative $\mathrm{D}\boldsymbol{p}_e/\mathrm{D}\widehat{\boldsymbol{F}}$ can be obtained, once an expression for the dependent sensitivity $\mathrm{D}\boldsymbol{h}_g/\mathrm{D}\widehat{\boldsymbol{F}}$ is found, since the sensitivies of the quantities at the previous time step are stored just like history variables and are therefore known. Please note, that this solution procedure requires design velocity fields for the sensitivities at the beginning of the analysis.

An equation determining the derivative $\mathrm{D}\boldsymbol{h}_g/\mathrm{D}\widehat{\boldsymbol{F}}$ is obtained by the total derivative of the dependent residual $\boldsymbol{Q}$ with respect to $\widehat{\boldsymbol{F}}$:

$$\frac{\partial \boldsymbol{Q}}{\partial \boldsymbol{p}_e}\frac{\mathrm{D}\boldsymbol{p}_e}{\mathrm{D}\widehat{\boldsymbol{F}}} + \frac{\partial \boldsymbol{Q}}{\partial \boldsymbol{h}_g}\frac{\mathrm{D}\boldsymbol{h}_g}{\mathrm{D}\widehat{\boldsymbol{F}}} + \frac{\partial \boldsymbol{Q}}{\partial {}^{n}\boldsymbol{p}_e}\frac{\mathrm{D}^{n}\boldsymbol{p}_e}{\mathrm{D}\widehat{\boldsymbol{F}}} + \frac{\partial \boldsymbol{Q}}{\partial {}^{n}\boldsymbol{h}_g}\frac{\mathrm{D}^{n}\boldsymbol{h}_g}{\mathrm{D}\widehat{\boldsymbol{F}}} + \frac{\partial \boldsymbol{Q}}{\partial \widehat{\boldsymbol{F}}} = \boldsymbol{0} \tag{42}$$

A rearrangement of this equation leads to

$$\frac{\mathrm{D}\boldsymbol{h}_g}{\mathrm{D}\widehat{\boldsymbol{F}}} = -\left(\frac{\partial \boldsymbol{Q}}{\partial \boldsymbol{h}_g}\right)^{-1}\left(\frac{\partial \boldsymbol{Q}}{\partial \boldsymbol{p}_e}\frac{\mathrm{D}\boldsymbol{p}_e}{\mathrm{D}\widehat{\boldsymbol{F}}} + \frac{\partial \boldsymbol{Q}}{\partial {}^{n}\boldsymbol{p}_e}\frac{\mathrm{D}^{n}\boldsymbol{p}_e}{\mathrm{D}\widehat{\boldsymbol{F}}} + \frac{\partial \boldsymbol{Q}}{\partial {}^{n}\boldsymbol{h}_g}\frac{\mathrm{D}^{n}\boldsymbol{h}_g}{\mathrm{D}\widehat{\boldsymbol{F}}} + \frac{\partial \boldsymbol{Q}}{\partial \widehat{\boldsymbol{F}}}\right) \tag{43}$$

In this equation, the derivative $\partial\boldsymbol{Q}/\partial\boldsymbol{h}_g$ is already known, as it is the tangent of the local Newton–Raphson procedure to determine the history variables. The following abbreviation is introduced to shorten expressions:

$$\boldsymbol{Z}_g = -\left(\frac{\partial \boldsymbol{Q}}{\partial \boldsymbol{h}_g}\right)^{-1}\left(\frac{\partial \boldsymbol{Q}}{\partial {}^{n}\boldsymbol{p}_e}\frac{\mathrm{D}^{n}\boldsymbol{p}_e}{\mathrm{D}\widehat{\boldsymbol{F}}} + \frac{\partial \boldsymbol{Q}}{\partial {}^{n}\boldsymbol{h}_g}\frac{\mathrm{D}^{n}\boldsymbol{h}_g}{\mathrm{D}\widehat{\boldsymbol{F}}} + \frac{\partial \boldsymbol{Q}}{\partial \widehat{\boldsymbol{F}}}\right) \tag{44}$$

Then, it follows that

$$\frac{\mathrm{D}\boldsymbol{h}_g}{\mathrm{D}\widehat{\boldsymbol{F}}} = \boldsymbol{Z}_g - \left(\frac{\partial \boldsymbol{Q}}{\partial \boldsymbol{h}_g}\right)^{-1} \frac{\partial \boldsymbol{Q}}{\partial \boldsymbol{p}_e} \frac{\mathrm{D}\boldsymbol{p}_e}{\mathrm{D}\widehat{\boldsymbol{F}}} \tag{45}$$

Now, this intermediate result is inserted into eq. (41), which gives us the definition of $\mathrm{D}\boldsymbol{p}_e/\mathrm{D}\widehat{\boldsymbol{F}}$:

$$\left(\frac{\partial \boldsymbol{R}_e}{\partial \boldsymbol{p}_e} - \frac{\partial \boldsymbol{R}_e}{\partial \boldsymbol{h}_g}\left(\frac{\partial \boldsymbol{Q}}{\partial \boldsymbol{h}_g}\right)^{-1} \frac{\partial \boldsymbol{Q}}{\partial \boldsymbol{p}_e}\right) \frac{\mathrm{D}\boldsymbol{p}_e}{\mathrm{D}\widehat{\boldsymbol{F}}} = -\left(\frac{\partial \boldsymbol{R}_e}{\partial \boldsymbol{h}_g}\boldsymbol{Z}_g + \frac{\partial \boldsymbol{R}_e}{\partial^n \boldsymbol{p}_e}\frac{\mathrm{D}^n \boldsymbol{p}_e}{\mathrm{D}\widehat{\boldsymbol{F}}} + \frac{\partial \boldsymbol{R}_e}{\partial^n \boldsymbol{h}_g}\frac{\mathrm{D}^n \boldsymbol{h}_g}{\mathrm{D}\widehat{\boldsymbol{F}}} + \frac{\partial \boldsymbol{R}_e}{\partial \widehat{\boldsymbol{F}}}\right) \tag{46}$$

The term in brackets on the left–hand–side of the equation can be recognized as the element stiffness matrix from the primal analysis (see [8]). Abbreviating the right–hand–side with the expression $-\tilde{\boldsymbol{R}}_e$, the equation is rewritten and gives

$$\boldsymbol{K}_e \frac{\mathrm{D}\boldsymbol{p}_e}{\mathrm{D}\widehat{\boldsymbol{F}}} = -\tilde{\boldsymbol{R}}_e \tag{47}$$

A standard assembly routine as it is used in the primal analysis leads to a global equation system which renders the sensitivities $\mathrm{D}\boldsymbol{p}_e/\mathrm{D}\widehat{\boldsymbol{F}}$ for the respective elements. The results can be inserted into eq. (43) to determine the dependent sensitivity.

The eqs. (38)–(47) were used to formulate an automatic differentiation based procedure for the actual evaluation of the intermediate variable $\boldsymbol{Z}_g$ and the dependent sensitivity pseudo–load vector $\tilde{\boldsymbol{R}}_e$ as described in [8]. The general symbolic tool AceGen [17] for automatic differentiation and automatic code generation was then used to implement the procedure.

This way, all the derivatives to determine the correct algorithmic tangent on the macrolevel $\widehat{\boldsymbol{A}}$ can be computed and the standard Newton–Raphson–scheme on the macro–level is applied with the correct tangent matrix. Thus, boundary value problems can be solved efficiently within a multiscale Finite–Element–framework, as shown in the next section.

4 NUMERICAL EXAMPLE

In this section, the bending of a beam consisting of inhomogeneous RVEs is investigated. The geometry and loading is illustrated in figure 2 (nodes on the left edge are fixed in position, nodes on the right edge are displaced vertically, measures are given in mm). The material data used for the computations are listed in table 1.

The vertical displacement and the distribution of the equivalent stress in the most upper and left RVE for an RVE–size of 0.01 mm x 0.01 mm are shown in figure 3.

Size effects can be observed when the size of the RVE is changed with respect to the size of the macrostructure and all material parameters are kept constant. In figure 4, the the Piola–stress P_{11} plotted over the logarithmic of the RVE–size is depicted as well as the force–displacement curves for varying RVE–sizes, where S is the length of one side of

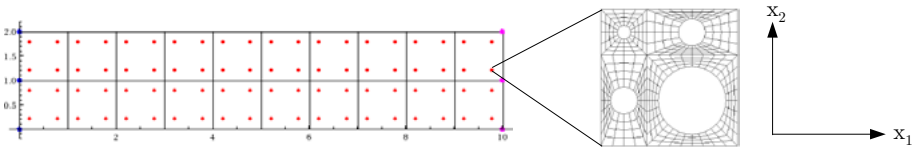

Figure 2: Bending of a beam with mesostructure

Table 1: Material parameters

μ	λ	K	τ_y	A	H
3571,4 MPa	14285,7 MPa	10 MPa	5 MPa	0.01 N	1000 MPa

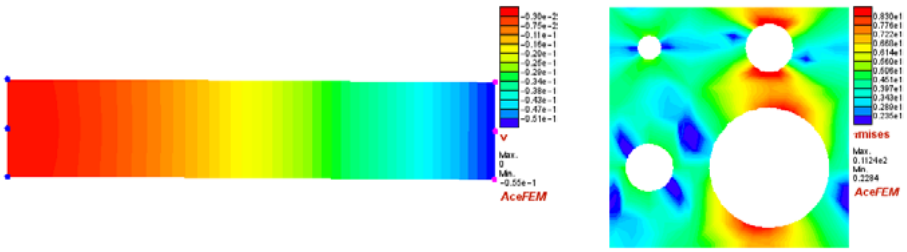

Figure 3: Displacement and stress distributions

the RVE. It is obvious, that the response is stiffer with decreasing RVE–size. This effect is also obtained by other homogenization schemes (see [18]).

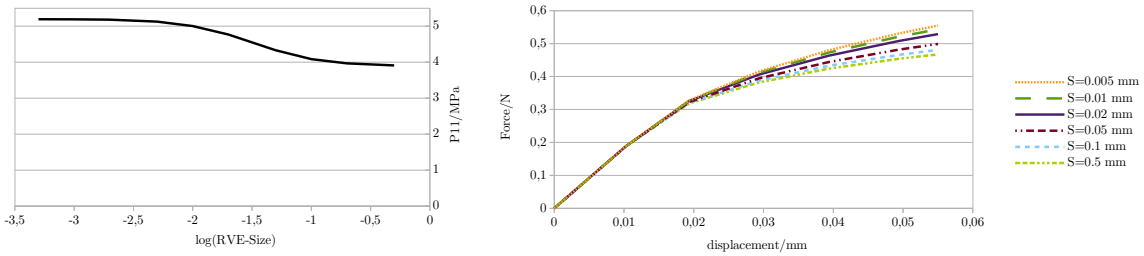

Figure 4: Size effects by variation of RVE–size

A second way to trigger size–effects is to change only A and to keep everything else constant. The results of the computations for different values of A are plotted in figure 5. It can be seen that a higher value of A leads to a stiffer response, which is in accordance to the results of single–scale computations of continua with inherent length scales.

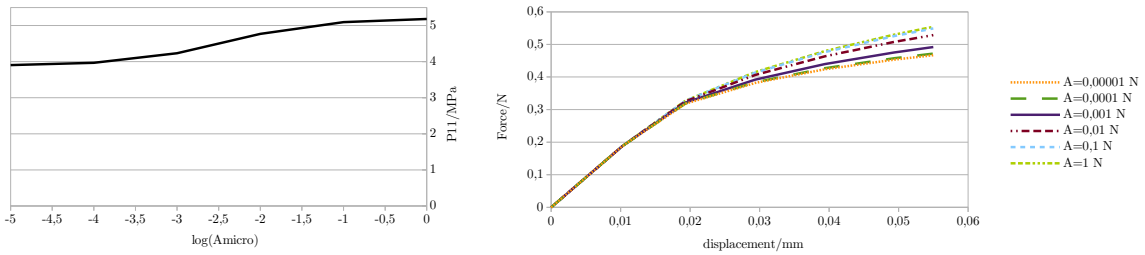

Figure 5: Size effects by variation of micro–stiffness A

5 CONCLUSION

In our work, we have described a two-scale computational homogenization method for finite elasto–plastic deformations. On the meso–level, a micromorphic–type model with an inherent length scale was used to model gradient–dependent material behavior capable of predicting size effects. It was shown, that the meso–to–macro transition fulfills the virtual work criterion and is thus physically meaningful. The algorithmic tangent of the time integration algorithm for the plastic evolution equations was homogenized exactly by means of sensitivity analyses. For this, the boundary conditions imposed on the RVE were used as sensitivity parameters. This nested solution procedure ensures quadratic convergence rates not only on RVE–level but also within the Newton–Raphson solution scheme on the macro–level.

This versatile and promising procedure can be easily extended to other history– and size–dependent problems such as micromorphic damage or tensorial micromorphic plasticity.

REFERENCES

[1] Voigt, W. Über die Beziehung zwischen den beiden Elasticitätskonstanten isotroper Körper. *Annalen der Physik und Chemie* (1889) **274**:573–587.

[2] Hashin, Z. Analysis of composite materials – A survey. *Journal of Applied Mechanics* (1983) **50**:481–505.

[3] Miehe, C., Schotte, J. and Schröder, J. Computational micro–macro transitions and overall moduli in the analysis of polycrystals at large strains. *Computational Materials Science* (1999) **16**:372–382.

[4] Miehe, C., Schröder, J. and Schotte, J. Computational homogenization analysis in finite plasticity. Simulation of texture development in polycrystalline materials. *Computer Methods in Applied Mechanics and Engineering* (1999) **171**:387–418.

[5] Féyel, F. Multiscale FE^2 elastoviscoplastic analysis of composite structures. *Computational Materials Science* (1999) **16**:344–354.

[6] Féyel, F. and Chaboche, J.–L. FE^2 multiscale approach for modelling the elastoviscoplastic behaviour of long fibre SiC/Ti composite materials. *Computer Methods in Applied Mechanics and Engineering* (2000) **183**:309–330.

[7] Simo, J.C. Algorithms for static and dynamic multiplicative plasticity that preserve the the classical return mapping schemes of the infinitesimal theory. *Computer Methods in Applied Mechanics and Engineering* (1992) **99**:61–112.

[8] Korelc, J. Automation of primal and sensitivity analysis of transient coupled problems. *Computational Mechanics* (2009) **44**:631–649.

[9] Michaleris, P., Tortorelli, D.A. and Vidal, C.A. Tangent operators and design sensitivity formulations for transient non–linear coupled problems with applications to elastoplasticity. *International Journal for Numerical Methods in Engineering* (1994) **37**:2471–2499.

[10] Hirschberger, C.B. and Steinmann, P. Classification of concepts in thermodynamically consistent generalized plasticity. *ASCE Journal of Engineering Mechanics* (2009) **135**:156–170.

[11] Eringen, A.C. *Microcontinuum Field Theories: I. Foundations and Solids*, Springer, (1999).

[12] Forest, S. Micromorphic approach for gradient elasticity, viscoplasticity and damage. *ASCE Journal of Engineering Mechanics* (2009) **135**:117–131.

[13] Clasen, H. and Hirschberger, C.B. On theory and computation of gradient–based multifield inelasticity. *Proceedings of the 6th European Congress on Computational Methods in Applied Sciences and Engineering (ECCOMAS 2012)*, (2012).

[14] Hill, R. On constitutive macro–variables for heterogeneous solids at finite strain. *Proceedings of the Royal Society London A* (1972) **326**:131–147.

[15] Hirschberger, C.B. and Sukumar, N. and Steinmann, P. Computational homogenization of material layers with micromorphic mesostructure. *Philosophical Magazine* (2008) **88**:3603–3631.

[16] Schröder, J. *Homogenisierungsmethoden der nichtlinearen Kontinuumsmechanik unter Beachtung von Stabilitätsproblemen*. Habilitation thesis, Stuttgart, (2000).

[17] Korelc, J. *AceGen user manual*. http://www.fgg.uni-lj.si/symech/, (2009).

[18] Kouznetsova, V., Geers, M.G.D. and Brekelmans, W.A.M. Multi–scale constitutive modelling of heterogeneous materials with a gradient–enhanced computational homogenization scheme. *International Journal for Numerical Methods in Engineering* (2002) **54**:1235–1260.